Extremely Pure Mg$_2$FeH$_6$ as a Negative Electrode for Lithium Batteries

Sergio Brutti [1,2] ⓘ**, Luca Farina** [3]**, Francesco Trequattrini** [1,4] ⓘ**, Oriele Palumbo** [1] ⓘ**, Priscilla Reale** [5] ⓘ**, Laura Silvestri** [3,5]**, Stefania Panero** [3,6] ⓘ **and Annalisa Paolone** [1,*] ⓘ

1   Consiglio Nazionale delle Ricerche, Istituto dei Sistemi Complessi, U.O.S. La Sapienza, Piazzale A. Moro 5, 00185 Roma, Italy; sergio.brutti@unibas.it (S.B.); francesco.trequattrini@roma1.infn.it (F.T.); oriele.palumbo@roma1.infn.it (O.P.)
2   Dipartimento di Scienze, Università della Basilicata, V.le Ateneo Lucano 10, 85100 Potenza, Italy
3   Dipartimento di Chimica, Sapienza Università di Roma, Piazzale A. Moro 5, 00185 Roma, Italy; luca.farina@uniroma1.it (L.F.); l.silvestri@uniroma1.it (L.S.); stefania.panero@uniroma1.it (S.P.)
4   Dipartimento di Fisica, Sapienza Università di Roma, Piazzale A. Moro 5, 00185 Roma, Italy
5   ENEA-Centro Ricerche Casaccia, via Anguillarese 301, 00123 Roma, Italy; priscilla.reale@enea.it
6   Research Center HYDRO-ECO, Sapienza University of Rome, Via A. Scarpa 14, 00161 Roma, Italy
*   Correspondence: annalisa.paolone@roma1.infn.it; Tel.: +39-6-4991-4400

Abstract: Nanocrystalline samples of Mg-Fe-H were synthesized by mixing of MgH$_2$ and Fe in a 2:1 molar ratio by hand grinding (MIX) or by reactive ball milling (RBM) in a high-pressure vial. Hydrogenation procedures were performed at various temperatures in order to promote the full conversion to Mg$_2$FeH$_6$. Pure Mg$_2$FeH$_6$ was obtained only for the RBM material cycled at 485 °C. This extremely pure Mg$_2$FeH$_6$ sample was investigated as an anode for lithium batteries. The reversible electrochemical lithium incorporation and de-incorporation reactions were analyzed in view of thermodynamic evaluations, potentiodynamic cycling with galvanostatic acceleration (PCGA), and ex situ X-ray Diffraction (XRD) tests. The Mg$_2$FeH$_6$ phase underwent a conversion reaction; the Mg metal produced in this reaction was alloyed upon further reduction. The back conversion reaction in a lithium cell was here demonstrated for the first time in a stoichiometric extremely pure Mg$_2$FeH$_6$ phase: the reversibility of the overall conversion process was only partial with an overall coulombic yield of 17% under quasi-thermodynamic control. Ex situ XRD analysis highlighted that the material after a full discharge/charge in a lithium cell was strongly amorphized. Under galvanostatic cycling at C/20, C/5 and 1 C, the Mg$_2$FeH$_6$ electrodes were able to supply a reversible capacity with increasing coulombic efficiency and decreasing specific capacity as the current rate increased.

Keywords: Mg$_2$FeH$_6$; reactive ball milling; high temperature hydrogenation; pressure-composition isotherms; discharge capacity

1. Introduction

The synthesis of Mg$_2$FeH$_6$ was reported for the first time in 1984 [1]. Since then, this compound has attracted large attention due to the peculiarities of this ternary system. One of them is the complete immiscibility of magnesium and iron in the binary phase diagram, surprisingly counterbalanced by the stability of a mixed ternary hydride [1]. Moreover, Mg$_2$FeH$_6$ displays the highest known volumetric hydrogen density among hydrides (150 kg·m^{-3}) and a considerable gravimetric capacity (5.4 mass %). The crystal structure of this compound is typical of a complex hydride [2–5]: hydrogen is located at the vertex of octahedra centered around Fe, and the [FeH$_6$]$^{4-}$ anions are bound to Mg^{2+} cations. The resulting crystalline solid has a cubic symmetry belonging to the F-3m space group [3].

The synthesis of magnesium iron hydride is usually obtained by means of two methods: (1) direct hydrogenation of Mg and Fe powders at high temperature and pressure; (2) reactive ball milling of Mg/Fe or MgH_2/Fe powders at room temperature, either in an inert or in a hydrogen atmosphere. In some cases, additional steps consisting of a hot extrusion process [6] or severe plastic deformation by ECAP (Equal Channel Angular Pressing) [7] were proposed. Quite recently, a solid state ball milling process followed by an additional wet ball milling process was exploited as a synthetic route [8]: the obtained samples consisted of a core of Mg_2FeH_6 (with a diameter of 40–60 nm) encapsulated within an outer shell of MgH_2 (5 nm thick), with superior dehydrogenation properties (~5.0 mass % H_2 released within 50 min at 280 °C).

In all cases, the obtained samples seem to be composed of a mixture of MgH_2 and Mg_2FeH_6 in various proportions; usually the concentration of the mixed hydride does not exceed 85 mass %. Only when the synthesis occurs at high temperature (450–520 °C) and pressure (20–120 bar), over a long time (several days) can one obtain a pure Mg_2FeH_6 sample [1].

Mg_2FeH_6 has been proposed in several applications. The most obvious is its use for solid state hydrogen storage: it was largely investigated by Bogdanovic et al. in samples obtained by direct hydrogenation of Fe and Mg or MgH_2 powders, with the proportion of the starting metals ranging from 1:2 to 1:40 [9]. The temperature dependence of the pressure plateau and the value of the enthalpy of hydrogenation/dehydrogenation (ΔH_{hydr} = 77.4 kJ/mol) were investigated. More recently, a prototype of hydrogen storage systems based on the magnesium iron hydride was reported [10].

The high value of ΔH_{hydr} makes Mg_2FeH_6 a suitable material for heat storage at relatively high temperatures (up to 550 °C) [11–13]. Indeed, during the discharge of hydrogen, the material absorbs heat, while the released H_2 can be stored for further use. Conversely, during hydrogen recharging, the stored heat can be used to generate electricity [10]. This process can be useful to compensate for fluctuations in the production from renewable energy sources, such as solar power plants [11]. Finally, magnesium iron hydride was proposed as an innovative negative electrode material for lithium batteries. Following the pioneering work of Oumellal et al. [14] showing the abilities of hydrides to undergo conversion reaction in lithium cells, the potential use of Mg_2FeH_6 as a negative electrode in Li cells was investigated. Zaïdi et al. [15] first demonstrated the ability of the mixed Mg and Fe hydride to electrochemically incorporate 6 lithium equivalents in a lithium cell (corresponding to a specific capacity of 1455 $mAhg^{-1}$) and to fully transform into a mixture of 2Mg + Fe + 6LiH through a conversion reaction. Moreover, Farina et al. showed that a partial reversibility (e.g., a coulombic efficiency of approximately 40%) can be obtained in samples produced by reactive ball milling starting from an overstoichiometric Mg-rich mixture of MgH_2 and Fe in a molar proportion 3:1 [16]. Additionally, the overpotentials were reported to be smaller after material activation by the H_2 sorption treatment at 400 °C [16].

In this paper, we investigate the electrochemical properties in lithium cells of an extremely pure Mg_2FeH_6 sample, obtained from MgH_2 and Fe in the stoichiometric ratio 2:1, ball milled in a hydrogen atmosphere. Our goal is to extend the knowledge of the conversion reaction of the Mg-Fe mixed hydride in lithium cells going beyond the state-of-the-art, in particular by investigating the lithium electrochemical extraction reaction (back conversion) and the reversible electrochemical activity of this phase.

2. Materials and Methods

Mg-Fe-H samples were produced by two different methods: (1) mixing of MgH_2 and Fe by hand grinding in an agate mortar (MIX); (2) by reactive ball milling (RBM) of MgH_2 and Fe in a high pressure vial by Evico Magnetics (Dresden, Germany) connected to a Fritsch Pulverisette P6 mill (Idar-Oberstein, Germany) under the following conditions: H_2 pressure 50 bar, ball to sample ratio 10:1, stainless steel ball diameter 6 mm, rotation speed 350 rpm in reverse mode, total milling time 40 h divided in cycles of 30 min milling and 5 min rest, temperature of the vial <31 °C (measured during

milling), mass of each batch ~3 g. The samples produced for this study are, therefore, MgH_2:Fe 2:1 molar ratio, produced either by mixing (Sample MIX) or by RBM (Sample RBM).

All samples, independent of the synthesis method, were produced starting from MgH_2 (hydrogen-storage grade) purchased from Sigma Aldrich (Saint Louis, MO, USA) and an Fe powder from Alfa Aesar (Haverhill, MI, USA). XRD diffraction patterns indicated that no iron oxides were present in the pristine Fe powder, at least within the experimental detection limits of this technique [17].

The XRD experiments were carried out in sealed capillary tubes, using a Rigaku X-ray Ultima+ diffractometer (Rigaku, Tokyo, Japan) equipped with a CuK_α source and a graphite monocromator for the diffracted beam. Apart from the initial powders, all the samples investigated by XRD were previously cycled in a hydrogen atmosphere at various temperatures in order to have maximum H_2 absorption.

Hydrogen sorption experiments were conducted in a custom-made Sieverts apparatus described elsewhere [18,19]. A mass in the range $0.3-0.5$ g was used for these measurements.

The samples morphology was investigated by transmission electron microscopy using an FEI Tecnai 200 kV cryo-TEM instrument (ThermoFisher Scientific, Waltham, MA, USA). In order to prevent possible damage due to the interaction of samples with the electron beam, experiments were carried out at 80 keV in a cryo-condition by cooling the sample holder with liquid nitrogen.

Electrochemical galvanostatic cycling tests were performed by means of a MACCOR 4000 Battery tester (Maccor, Tulsa, OK, USA). Pelletized electrodes were realized with composite mixtures of the active material hand ground with the typical additives: Timcal Super P carbon electron conductor and Kynar 20810 PVdF binder (Arkema, Colombes, France) in a 5:3.2 ratio. Powders were spread on a copper disk (10 mm in diameter) inside a Specac$^{®}$ (Orpington, UK) die set and pelletized by using a hydraulic press (10 tons). The resulting pellet was strongly coated onto the copper. The typical mass loading of the electrodes ranged between 1.0–2.5 mg·cm^{-2}. The electrode preparation procedure was carried out in an Ar-filled glove box. Electrochemical cells were assembled facing the Mg_2FeH_6 electrode with metallic lithium foil (Chemetall, Frankfurt, Germany), with two Whatmann separators in between and soaked by a 1 M $LiPF_6$ solution in ethylene carbonate and dimethylcarbonate 1:1 w/w mixture (Merck Selectipur, Darmstadt, Germany). Cycling tests were performed at various current rates (1 C = 1455 mA/g; 1 Li eq = 242.5 mAhg^{-1}) in the 0.01–2.5 V voltage range. For potentiodynamic cycling with galvanostatic acceleration (PCGA) tests, three electrode electrochemical cells were assembled by facing the working electrode to a lithium metal foil counter through a Whatman borosilicate fiber separator (Sigma Aldrich, Saint Louis, MO, USA) swollen with the electrolyte. The lithium reference electrode was placed perpendicularly to the assembly, soaked by an electrolyte excess. In order to collect potential profiles negligibly affected by overpotentials, thus under quasi-thermodynamic control, PCGA tests were carried out by means of a Biologic VSP potentiostat (Bio-Logic Science Instruments, Seyqssinet-Pariset, France), in the potential range of 2.5–0.01 V, with 10 mV steps and a cutoff current equal to C/20, calculated as the current to deliver in 20 h the full theoretical conversion capacity.

Ex situ XRD experiments were performed by recuperating electrode materials from the electrochemical cells following our standard procedure outlined in ref. [16]. Samples were sealed in capillary tubes and XRD patterns were recorded, using a Rigaku X-ray Ultima+ diffractometer equipped with a CuK_α source and a graphite monocromator for the diffracted beam.

All handling of the samples was performed in a glove-box by Jacomex (O_2 and H_2O levels lower than 0.1 pm) (Jacomex, Dagneux, France), both for electrochemical tests and for Sieverts measurements. Thanks to these experimental conditions, the samples here investigated were never exposed to air.

3. Results and Discussion

3.1. Phase Formation under H_2

The first aim of the present study was to measure the concentration of MgH_2 and Mg_2FeH_6 in the samples produced either by mixing or by reactive ball milling, and subsequently hydrogenated at different temperatures. Therefore, we performed pressure-composition measurements at various temperatures between 340 and 485 °C (see Figure 1). The investigated pressure spanned the range 0.1–100 bar. For sample MIX, the dehydrogenation isotherms were measured at all temperatures. By contrast, for the sample RBM, the dehydrogenation isotherms were collected at each temperature, while the absorption isotherms were obtained only at 340 and 400 °C, due to the extremely slow kinetics of the absorption process under near-equilibrium conditions.

For sample MIX, one observes that at all temperatures the isotherms are composed of two pressure plateaus, labeled as A and B in Figure 1. Plateau A is centered at a higher pressure and its width shrinks as temperature increases. The absolute pressure value of plateau A is compatible with that of MgH_2 [16]. On the contrary, Plateau B, centered at lower pressure, expands as T increases; the absolute value of the pressure of plateau B is compatible with that measured for Mg_2FeH_6 [9,16]. One can observe that increasing T, the total amount of hydrogen stored in the sample increases, starting from ~3.8 wt % at 340 °C and reaching ~4.9 wt % at 485 °C.

A similar behavior is found for Sample RBM; however, in this case, at the highest temperature (485 °C), plateau A practically disappears and only plateau B persists. Moreover, the total amount of hydrogen stored in Sample RBM at 485 °C is ~5.4 wt %, as expected for pure Mg_2FeH_6.
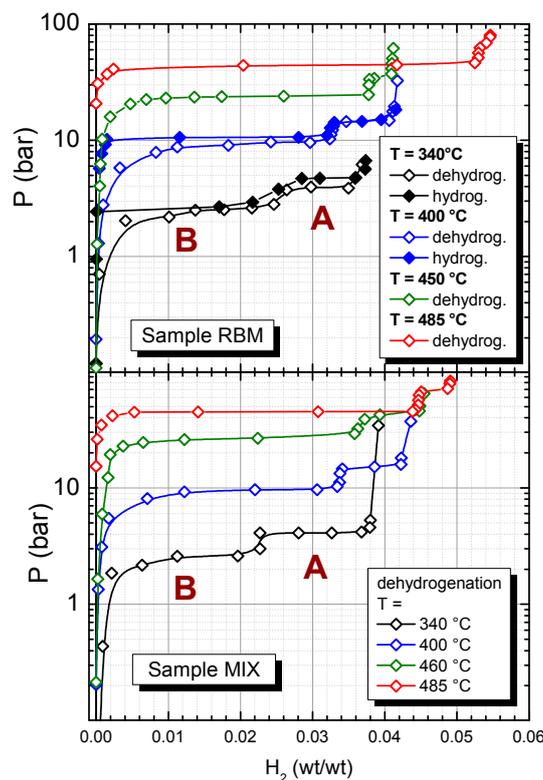

Figure 1. Pressure-composition isotherms of Sample RBM and Sample MIX at various temperatures.

From the width of the plateaus at the various temperatures, knowing that the maximum hydrogen capacity of MgH_2 and Mg_2FeH_6 is 7.6 and 5.4 wt %, respectively, one can easily calculate the amount of each phase in the sample (see Table 1). As nicely detectable in Figure 1, in Sample MIX the amount of MgH_2 decreases from 43% at 340 °C to 11% at 485 °C, while the concentration of Mg_2FeH_6

increases from 46% at 340 °C to 83% at 485 °C. Similar figures are obtained for Sample RBM; however, in the case of the sample produced by the reactive ball milling method, at 485 °C one obtains an amount of $Mg_2FeH_6 > 97\%$, i.e., the sample cycled at this temperature is practically a pure sample of magnesium-iron hydride. For the sample MIX, we could not obtain a sample of pure magnesium-iron hydride, even after cycling at the highest temperature (485 °C). Possibly the reduction of the size of the iron particles induced by the ball milling allows a more intimate mixing of Mg and Fe, which should diffuse at a much lower distance in order to give rise to Mg_2FeH_6 upon hydrogenation.

It can be noted in Table 1 that, no matter how the synthesis is carried out, part of the material remains unreacted, since the total amount of the MgH_2 and Mg_2FeH_6 phases does not reach the 100% of the total sample, apart for sample RBM cycled at 485 °C. Moreover, the amount of hydrogen stored in the compounds is slightly higher in sample MIX than in Sample RBM for $T \leq 460$ °C. The observation of a mixture of MgH_2 and Mg_2FeH_6 for samples obtained by hydrogen cycling or reactive ball milling of MgH_2 (or Mg) and Fe is not new, as it is a well established property of this system. Indeed, Bogdanovic et al. [9] reported p-c isotherms for compounds synthesized with 2:1 or 4:1 Mg:Fe molar ratios; both of them exhibited two pressure plateaus corresponding to the hydrogenation/dehydrogenation of Mg_2FeH_6 and MgH_2. However, to the best of our knowledge, systematic investigations of the thermal evolution of the concentration of the two hydrides are extremely rare. In the case of a non-stoichiometric mixture obtained by reactive ball milling of MgH_2 and Fe in a molar ratio 3:1, we previously reported such information [16], obtained again from pressure-composition isotherms. Also, in the non-stoichiometric mixture, the amount for magnesium-iron hydride increases as temperature increases: the sample was reported to be composed of ~30% MgH_2 and ~44% Mg_2FeH_6 at 335 °C, and of ~24% MgH_2 and ~54% Mg_2FeH_6 at the maximum investigated temperature of 390 °C [16]. More recently [20], Witek et al. reported that sintering samples obtained from MgH_2 and Fe under stoichiometric concentration at 500 °C yielded the ternary hydride with a yield higher than 90%, independent of the milling conditions. Aselli et al. reported the relative quantities and crystallite size of phases identified in ball milled samples as calculated by Rietveld refinement [21]. Also, in the present case, XRD patterns for the RBM and MIX cycled at 485 °C (Figure 2) confirmed that they were almost completely constituted by the ternary hydride with minor residual metal iron.

Table 1. Composition of samples (at %) cycled at various temperatures, calculated from the pressure composition isotherms reported in Figure 1.

Sample Name	Composition at 335 °C		Composition at 385 °C		Composition at 450 °C		Composition at 485 °C	
	MgH_2	Mg_2FeH_6	MgH_2	Mg_2FeH_6	MgH_2	Mg_2FeH_6	MgH_2	Mg_2FeH_6
RBM	30%	46%	25%	59%	8%	70%	<3%	>97%
MIX	43%	41%	22%	63%	24%	67%	11%	83%

Both the MIX and the RBM materials after sorption at 485 °C are constituted by a mixture of two well crystallized phases, i.e., Mg_2FeH_6 and metallic Fe. This evidence is in good agreement with the residual amount of MgH_2 highlighted in the pressure composition isotherms for both the MIX and RBM materials. The diffraction lines of the MgH_2 phase are absent, possibly due to a strong amorphization or nanometrization. Tentative Rietveld refinements, performed considering the presence of the Mg_2FeH_6 and metallic Fe phases only, allow us to estimate the relative amounts of the constituent phases in each material (MIX at 485 °C: at % $(Mg_2FeH_6) = 95 \pm 1\%$ at %(Fe) = $5 \pm 1\%$ wRp = 0.075; RBM at 485 °C: at % $(Mg_2FeH_6) = 97 \pm 1\%$ at % (Fe) = $3 \pm 1\%$ wRp = 0.064). These estimates matches those calculated from the pressure composition isotherms reported in Table 1.
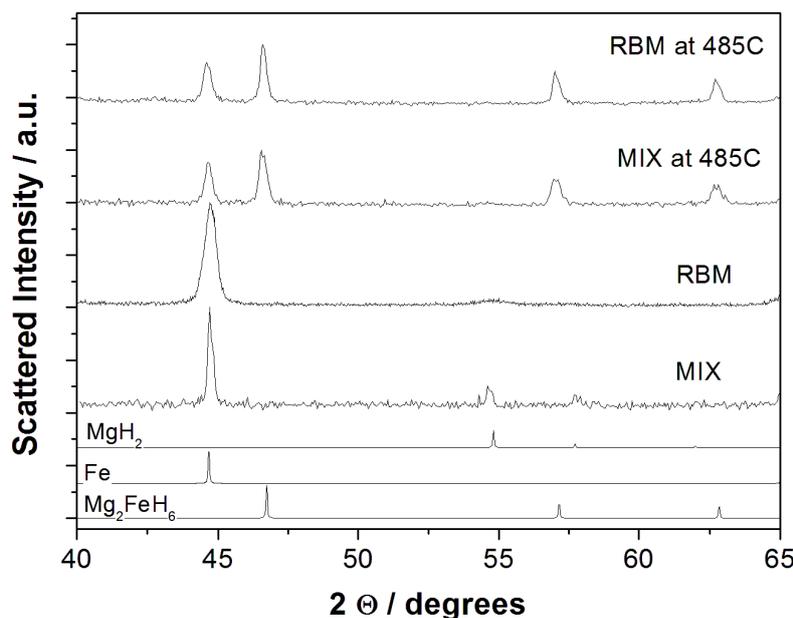
Figure 2. XRD patterns of the RBM and MIX samples before hydrogen sorption and after H_2 sorption at 485 °C.

From the pressure-composition isotherms reported in Figure 1, the dehydrogenation enthalpy, ΔH_{dehydr}, and entropy, ΔS_{dehydr}, of Mg_2FeH_6 can be obtained, by means of the well known van't Hoff equation, by plotting the logarithm of the plateau pressure as a function of the inverse of the temperature; the slope of the graph provides ΔH_{dehydr}, while the intercept gives ΔS_{dehydr}. From the present data, one obtains ΔH_{dehydr} = 77 ± 2 kJ/mol or 76.0 ± 0.6 kJ/mol for Sample MIX and Sample RBM, respectively. These values are in agreement within the estimated accuracies and compare well with that reported by Bogdanovic et al. (77.4 kJ/mol) [9]. Moreover, for the first time we obtained a value of the dehydrogenation entropy for Mg_2FeH_6: ΔS_{dehydr} = 131 ± 1 kJ/(mol·K) or 133 ± 2 kJ/(mol·K) for Sample MIX and Sample RBM, respectively. These values are comparable with those usually obtained for metal hydrides, which range between ~68 J/(mol·K) of LiH, 133.4 ± 0.7 J/(mol·K) of MgH_2 and 157 J/(mol·K) of SrH_2 [22].

The morphologies of the two series of samples, i.e., RBM and MIX, before and after the hydrogen sorption were also investigated by TEM and are shown in Figure 3. The two materials, MIX and RBM, before hydrogen sorption show a very different morphology. The MIX sample is constituted by large round-shaped dense particles, likely metallic iron, mixed with irregular less dense particles, constituted by lighter elements possibly due to MgH_2 aggregates. On the other hand, the RBM sample shows composite aggregates constituted by a light matrix that incorporates small, dark dense particles. The evolution of the morphology of both samples after hydrogen sorption is similar. In fact both the MIX and the RBM samples after hydrogen sorption at 450 °C and at 485 °C are constituted of smooth particles with irregular shapes and a homogeneous contrast, thus indicating the strong interaction between the two original constituents observed in the XRD patterns and highlighted by the pristine morphology. As expected, the size of these irregular smooth particles increases at 485 °C compared to 450 °C for both the RBM and the MIX materials. Between the two series of materials, apparently the only main difference in the morphology after hydrogen sorption is a slightly larger particle size observed in the MIX samples compared to the RBM ones.
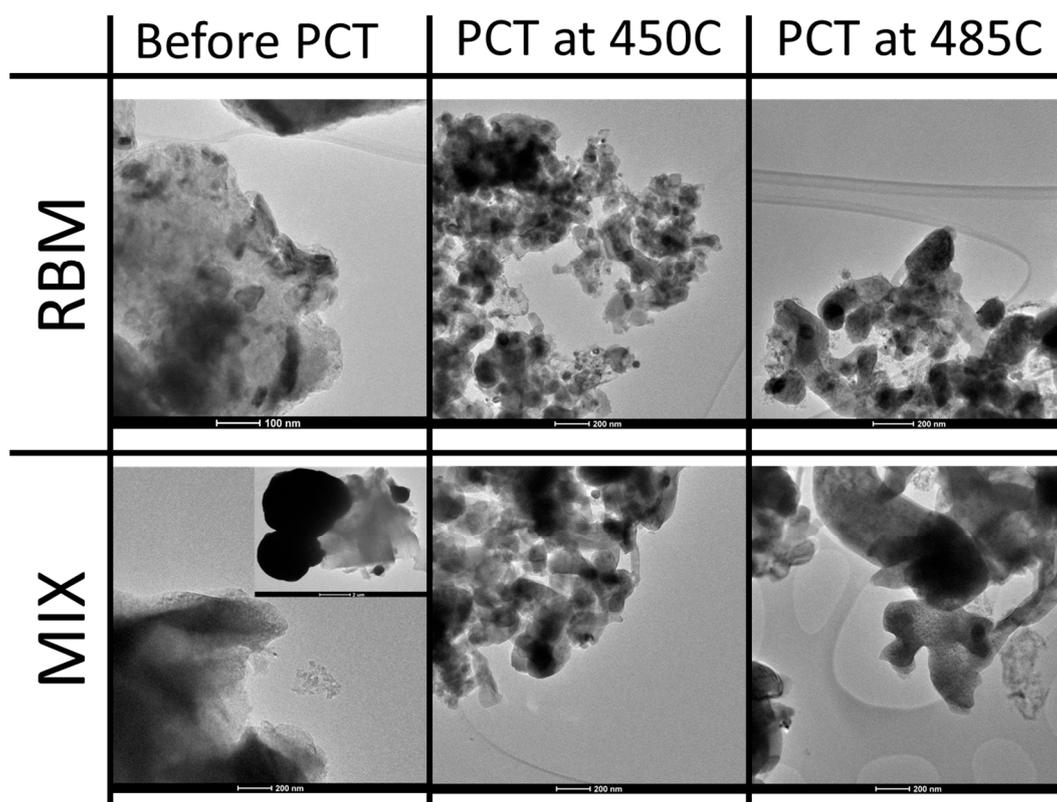
Figure 3. Evolution of the morphology for the two series of samples, i.e., RBM and MIX, before hydrogen sorption and after H_2 sorption at two temperatures.

Overall, the synthesis of very pure Mg_2FeH_6 phases starting from a stoichiometric mixture of the reagents necessitates a ball milling stage. This finding is expected, but the extent of the residual amount of unreacted Fe/MgH_2 in the MIX sample is remarkable and worth noting. In fact our data highlight that the synthesis to a Mg_2FeH_6 phase with unreacted Fe/MgH_2 impurities <5% requires a mechanochemical activation of the starting reagents under 50 bar of hydrogen, despite the subsequent drastic treatment at 485 °C under 100 bar of hydrogen gas.

3.2. Electrochemical Characterization

Mg_2FeH_6 was investigated as a negative electrode for lithium ion cells. According to the full conversion reaction mechanism studied in [15], the Mg_2FeH_6 phase can supply a theoretical specific capacity of 1455 mAhg^{-1} through the reaction $Mg_2FeH_6 + 6Li^+ + 6e^- \rightarrow 2Mg + Fe + 6LiH$. Besides this preliminary analysis by Zaïdi et al. [15], to the best of our knowledge, the multiple redox processes of pure Mg_2FeH_6 in lithium cells were never investigated in detail and in particular, the analysis of the back-conversion reaction has never been attempted.

The electrochemical incorporation/de-incorporation of lithium in the Mg_2FeH_6 phase under quasi-thermodynamic conditions was investigated, in the present work, by PCGA as shown in Figure 4 for the RBM sample cycled in the Sieverts apparatus at 485 °C.
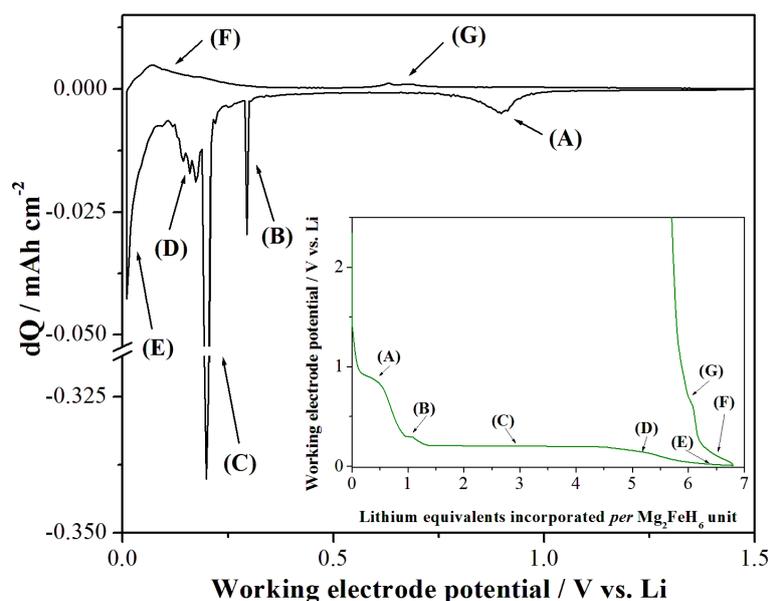
Figure 4. Differential capacity plot obtained in the PCGA test performed on the Mg_2FeH_6 material (RBM sample after H_2 sorption at 485 °C) (composite electrode: AM:SP:Binder = 5:3:2). In the inset, the corresponding lithium loading/extraction curves are shown. Labels (A) to (G) identify the occurrence of electroactive processes.

Five different consecutive electroactive processes can be observed under reduction (labeled from A to E in Figure 4) and two upon oxidation (F and G). Besides process (A) that is likely due to the decomposition of the electrolyte and the solid electrolyte interphase formation [23], processes (B), (C) and (E) show a stable potential plateau. On the contrary, reactions (D), (F) and (G) show potential slopes. This evidence may suggest the occurrence of a complex lithium incorporation/de-incorporation mechanism.

In order to shed light on this multistep process, a summary of the possible conversion/alloying reactions in the Mg-Fe-H system is presented in Table 2. The reaction thermodynamics (i.e., $\Delta_r G°_{298K}$, Gibbs energy of reaction at 298 K) of processes (1) to (6) have been calculated starting from the Gibbs energy of formations of Mg_2FeH_6 [24], MgH_2 [25], LiH [26], Li_xMg(hcp) and Li_yMg(bcc) [27] available in the literature (in the case of Mg_2FeH_6, the literature data were also averaged with our data discussed above). The corresponding Nernst redox potential was derived by the equation $\Delta E° = -n \times F \times \Delta_r G°_{298K}$, where n is the total number of exchanged electrons and F is the Faraday constant. It is important to recall that, as Li_xMg(hcp) and Li_yMg(bcc) are two solid solutions, their thermodynamic formation properties vary with the lithium stoichiometry and, therefore, the Nernst Redox potentials of the alloying reactions (4) and (6) decrease with the increase of the lithium content.

Table 2. Thermodynamic analysis of the conversion reactions of the Fe-H-Mg phases.

	Electrochemical Reaction	Mechanism	Nernst Redox Potential V vs. Li	Ther. Loading Curve Shape	Theor. Li Loading per Mole of Reagent
(1)	$Mg_2FeH_6 + 2Li^+ + 2e^- \rightarrow 2MgH_2 + Fe^0 + 2LiH$		0.533	Plateau	2
(2)	$Mg_2FeH_6 + 6Li^+ + 6e^- \rightarrow 2Mg(hcp)^0 + Fe^0 + 6LiH$	Multi-phases conversions	0.527	Plateau	6
(3)	$MgH_2 + 2Li^+ + 2e^- \rightarrow Mg(hcp)^0 + 2LiH$		0.524	Plateau	2
(4)	$Mg(hcp)^0 + xLi^+ + xe^- \rightarrow Li_xMg(hcp)$ x < 0.15	**Single-phase alloying**	0.242 (x = 10^{-4}) 0.125 (x = 0.01) 0.063 (x = 0.15)	Slope	0.15
(5)	$Li_{0.15}Mg(hcp) + 0.2Li^+ + 0.2e^- \rightarrow Li_{0.35}Mg(bcc)$	Two-phase alloying	0.052	Plateau	0.2
(6)	$Li_{0.35}Mg(bcc) + yLi^+ + ye^- \rightarrow Li_{0.35+y}Mg(bcc)$	Single-phase alloying	0.040 (x = 10^{-4}) 0.037 (x = 0.01) 0.008 (x = 0.10)	Slope	y

From the thermodynamic point of view, the electrochemical lithium incorporation reaction starting from Mg_2FeH_6 should follow the reaction sequence (1)-(3)-(4)-(5)-(6). This sequence implies the incorporation of (2 + 2 × (2 + 0.15 + 0.2 + y) = 6.7 + 2y) lithium equivalents per mole of Mg_2FeH_6. It is interesting that the direct occurrence of reaction (2) is thermodynamically unfavorable.

In Table 3, a tentative matching between the experimental results obtained in the PCGA test and the thermodynamic evaluations summarized in Table 2 is presented.

Table 3. Composition of samples cycled at various temperatures, calculated from the pressure composition isotherms reported in Figure 1.

Range (See Figure 4)	Mean Electrode Potential V vs. Li	Lithium Loading Curve Shape	Experimental Li Equivalents Exchanged per Mg_2FeH_6 Unit	Tentative Identification of the Electrochemical Reaction
(A)	0.901	Slope	0.88	Solid electrolyte interphase formation
(B)	0.295	Plateau	0.41	(1)
(C)	0.199	Plateau	3.29	(2) or (1) + (3)
(D)	0.161	Slope	0.93	See discussion
(E)	0.020	Pseudo-Plateau	1.28	
(F)	0.070	Slope	0.63	(4), (5), (6)
(G)	0.0629	Slope	0.36	(1), (2), (3)

As already mentioned, the electrochemical process in the (A) range (see Figure 4) is likely due to the SEI-formation in agreement with the literature [23] also for the MgH_2 hydride [28]. The two following electroactive processes occur through one short (B) and one extended (C) potential plateau, both compatible with the occurrence of reactions (1) or (2) with moderate overvoltages (0.2–0.3 V) [29].

From a quantitative point of view, starting from an almost pure Mg_2FeH_6 material (moles of MgH_2 < 3% estimated from the Sievert measurements, see above), the short plateau (B), possibly attributed to reaction (1), leads to a mixture of ~80% Mg_2FeH_6 and ~20% MgH_2. The lithium loading curve further evolves with a limited slope, likely due to increasing overvoltages affecting reaction (1), and then stabilizes in a prolonged potential plateau (C) possibly attributed to reaction (2), or the simultaneous occurrence of reactions (1) and (3). By neglecting the lithium loaded in region (A), at the end of plateau (C) the incorporated lithium equivalents are 3.7 per Mg_2FeH_6 formula unit, to be compared to the 6 equivalents theoretically achievable. Apparently, the conversion reaction is incomplete and only 62% of the starting reagent is electrochemically reduced at the end of these two plateaus.

Going beyond the (B) and (C) plateaus, the lithium loading curve follows a slope (D) and a pseudo-plateau (E), down to the 10 mV potential cutoff. These additional processes show potential profiles similar to the alloying reactions into the Mg lattices (hcp or bcc) already demonstrated by us at the end of the conversion reaction of MgH_2 in lithium cells [28]. Our thermodynamic analysis suggests the occurrence of a sequence of three reactions: (4) the mono-phasic lithium loading into the hcp lattice of metallic Mg; (5) the bi-phasic transformation from $Li_{0.15}Mn$(hcp) to $Li_{0.35}Mg$(bcc) and (6) the mono-phasic lithium incorporation into the bcc lattice of the Mg-Li solid solution. However, the amount of lithium electrochemically incorporated in region (D) and (E) (i.e., 0.93 and 1.28 equivalents per Mg_2FeH_6 unit) exceeds that expected by the occurrence of reactions (4) and (5) (i.e., 0.19 and 0.25 equivalents per Mg_2FeH_6 unit assuming a 62% yield for the conversion reaction, see above). Owing to this, and considering the incompleteness of the conversion reaction at higher potentials, our interpretation is that at potentials < 0.2 V vs. Li, complex reactions occur simultaneously, likely including conversions (1-2-3) with increasing overvoltages and lithium alloying (4-5-6) in the Mg lattice. We would like to stress that the alloying reaction is unfortunately only postulated since the electrochemical data do not allow a straightforward identification of the underlying solid state reactivity. Toward this aim, in-operando spectroscopic studies would be useful to confirm this phenomenon; at present this approach is beyond our experimental capabilities.

Turning to the charge processes, it is possible to identify two well separated regions (F) and (G). Based on thermodynamic considerations, these processes can be attributed to the de-alloying reactions from the lithiated Mg lattices and the back conversions.

Overall, the lithium de-incorporation reactions under quasi-thermodynamic control have poor yields compared to the conversion/alloying observed upon discharge, being the coulombic efficiency approximately 0.17, excluding the lithium loading in the region (A) due to the SEI formation.

Ex situ XRD was carried out on an electrode after a full discharge and re-charge cycle in order to verify which hydride is experimentally formed upon recharge, i.e., Mg_2FeH_6 or MgH_2. Figure 5 compares the patterns of the cycled electrode to the pristine electrode. Despite the fact that the copper support signal dominates the pattern after 1 cycle, only very small diffraction peaks due to metallic iron particles and the pristine Mg_2FeH_6 phase are present. Apparently, no diffraction peaks related to MgH_2 or Mg can be highlighted. This evidence suggests that upon reduction/oxidation the material undergoes severe nanometrization, and that no crystalline hydrides are formed either after reduction or oxidation. It is interesting to underline the absence of peaks due to the metallic iron after 1 discharge/charge cycle. This effect can be a clue to the possible occurrence of a back conversion upon oxidation to amorphous Mg_2FeH_6.

The irreversible amorphization of the Mg_2FeH_6 electrode upon reduction/oxidation is in contrast to similar XRD analyses performed by us on $NaAlH_4$ and MgH_2 where the pristine hydride lattice re-crystallizes after a full discharge/charge process [28,30].
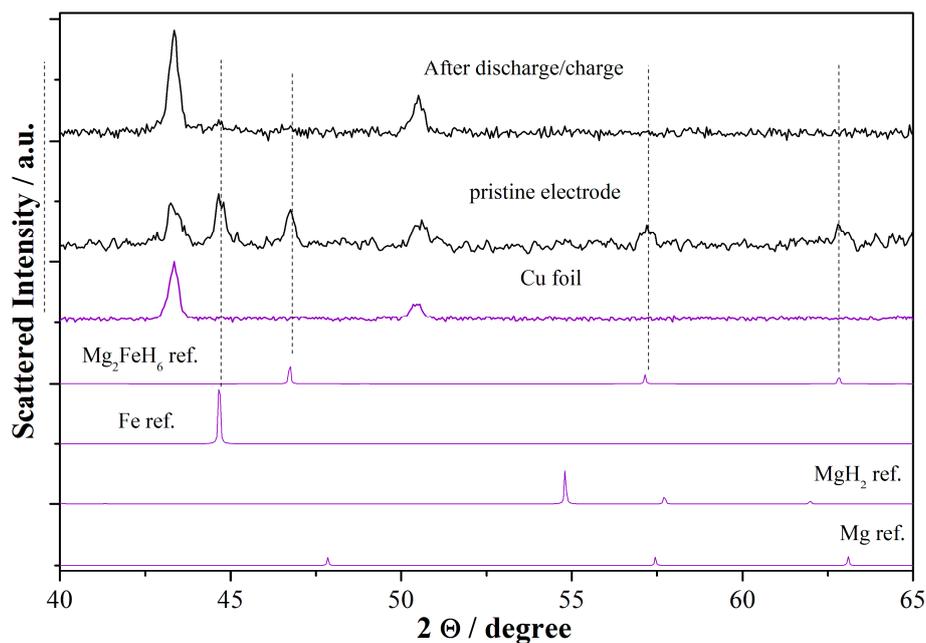

Figure 5. XRD patterns of the RBM electrode recorded after 1 galvanostatic cycle in lithium cells compared to the pristine material and references.

As a final point, it is important to recall the possible extra capacity supplied at low potential by the reversible formation/decomposition of a polymer/gel-like film promoted by the highly reactive metallic nanograins formed during conversion [31]. Laruelle et al. evaluated the reversible capacity provided by this reversible parasitic reactivity occurring in parallel with the electrochemical CoO/Co conversion reaction [31]. On this basis evaluation, although highly speculative, we may estimate in the case of the Mg_2FeH_6 phase a possible contribution due to the electrolyte degradation at low potential as high as 8% of the first discharge capacity. Sample RBM cycled in the Sieverts apparatus at 485 °C was also electrochemically tested in lithium cells under galvanostatic conditions and at various current rates to evaluate the reversibility and cycling ability of this material. Results are shown in Figure 6.
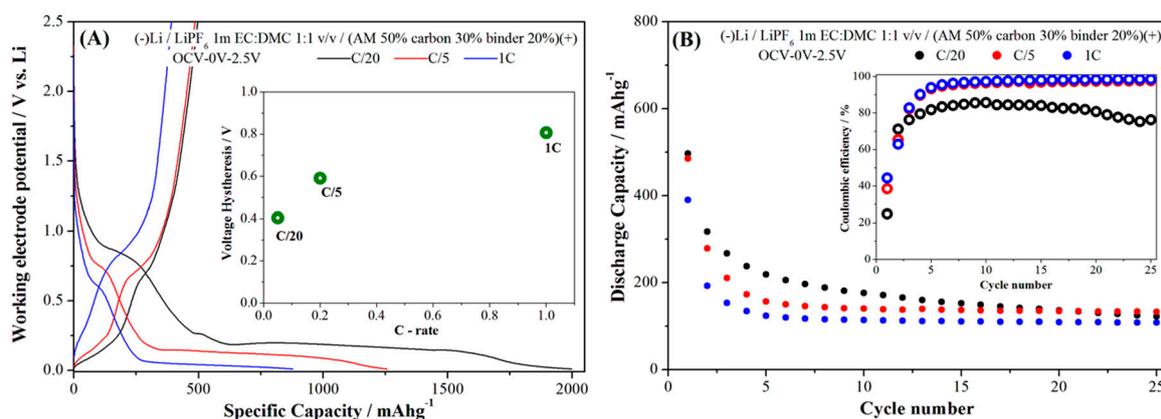
Figure 6. (**A**) Voltage profile of Mg_2FeH_6 (RBM sample after H_2 sorption at 485 °C) obtained upon discharge and following re-charge in a lithium cell (in the (a-inset) the voltage hysteresis vs. the C-rate is shown) (**B**) specific capacity measured upon cycling at various current rates (RBM sample after H_2 sorption at 485 °C); in the (b-inset) the trend of the coulombic efficiencies are shown).

Generally speaking, the RBM sample, which is constituted by almost pure Mg_2FeH_6 is able to allow a partially reversible lithium incorporation/deincorporation in the first cycle and fading capacities upon cycling. The measured performance is in line with our previous observation of $(3MgH_2 + Fe)$ composites [16] but, as far as we know, this is the first ever reported evidence of a prolonged reversible galvanostatic cycling of an almost pure Mg_2FeH_6 material. In reference [30] we estimated the capacity possibly provided by the SuperP additive upon cycling in $NaAlH_4$/superP/PVdF electrodes (5:3:2 ratio). Similar evaluations applied to the present Mg_2FeH_6 case would suggest a maximum contribution of the SuperP additive smaller than 5% of the overall capacity in the first discharge and not larger than 15% at cycle 10.

Turning to the experimental rate performance, the first discharge capacity, as well as the overall performance, decreases at increasing current rate due to the larger overpotentials, whereas the coulombic efficiencies increase. In particular, it is interesting to observe the quite large hysteresis between discharge/charge mean working voltages that exceeds 400 mV for all current rates. Among hydrides, these voltage hysteresis are remarkably large, in particular with respect to the small values measured by us for the conversion reaction of MgH_2 [28,29].

4. Conclusions

In this paper, we investigated the electrochemical properties in lithium cells of an extremely pure Mg_2FeH_6 sample. Nanocrystalline samples of Mg-Fe-H were synthesized by mixing of MgH_2 and Fe in a 2:1 molar ratio by hand grinding (MIX) or by reactive ball milling (RBM) in a high-pressure vial. Hydrogenation procedures were performed at various temperatures in order to promote the conversion to Mg_2FeH_6. XRD and Sieverts analyses suggest that pure Mg_2FeH_6 is obtained only for the RBM material cycled in hydrogen at 485 °C. This material was investigated as an anode for lithium batteries. The reversible electrochemical lithium incorporation and de-incorporation reactions were studied by PCGA and ex situ XRD tests. Thermodynamic evaluations were discussed in view of the experimental results. The Mg_2FeH_6 phase underwent a conversion reaction, and the produced Mg metal particles could be alloyed upon further reduction. The electrochemical reversibility of the conversion process in lithium cells was demonstrated here for the first time in the literature on stoichiometric Mg_2FeH_6 samples. However, even under quasi-thermodynamic control, the back oxidation was only partial with an overall coulombic yield of 17%. The material after a full discharge/charge in a lithium cell was strongly amorphized. The RBM material cycled in hydrogen at 485 °C in galvanostatic cycling at C/20, C/5 and 1 C was able to supply a reversible capacity exceeding in all cases 400 mAhg^{-1} in the

first cycle. The coulombic efficiencies and the specific capacities upon cycling followed the expected opposite trend while increasing the current rate.

Overall, our findings extend the previous observation concerning the Mg_2FeH_6 conversion mechanism in lithium cells reported by Zaidi et al. [15] by demonstrating the partial reversibility of the conversion reaction and the apparent irreversible amorphization of the electrode constituent after one full discharge/charge cycle.

Author Contributions: Conceptualization, S.B., P.R., S.P. and A.P.; Data curation, S.B., L.F., F.T., O.P., L.S. and A.P.; Writing original draft, S.B. and A.P.

Conflicts of Interest: The authors declare no conflict of interest.

References

1. Didisheim, J.J.; Zolliker, P.; Yvon, K.; Fischer, P.; Schefer, J.; Gubelmann, M.; Williams, A.F. Dimagnesium iron(II) hydride, Mg_2FeH_6, containing octahedral FeH_6^{4-} anions. *Inorg. Chem.* **1984**, *23*, 1953–1957. [CrossRef]

2. Retuerto, M.; Alonso, J.A.; Martínez, R.; Jiménez-Villacorta, F.; Sánchez-Benítez, J.; Fernández-Díaz, M.T.; Garcia-Ramos, C.A.; Ruskov, T. Neutron Powder Diffraction, X-ray absorption and Mössbauer spectroscopy on Mg_2FeH_6. *Int. J. Hydrogen Energy* **2015**, *40*, 9306–9313. [CrossRef]

3. Lang, J.; Fritzche, H.; Asselli, A.A.C.; Huot, J. In-situ In-situ neutron diffraction investigation of Mg_2FeH_6 dehydrogenation. *Int. J. Hydrogen Energy* **2017**, *42*, 3087–3096. [CrossRef]

4. Miwa, K.; Takagi, S.; Matsuo, M.; Orimo, S.-I. Thermodynamical stability of complex transition metal hydrides Mg_2FeH_6. *J. Phys. Chem. C* **2013**, *117*, 8014–8019. [CrossRef]

5. Chaudhary, A.-L.; Dietzel, S.; Li, H.-W.; Akiba, E.; Bergemann, N.; Pistidda, C.; Klassen, T.; Dornheim, M. Synthesis of Mg_2FeD_6 under low pressure conditions for Mg_2FeH_6 hydrogen storage studies. *Int. J. Hydrogen Energy* **2017**, *42*, 11422–11428. [CrossRef]

6. De Lima, G.F.; Garroni, S.; Baró, M.D.; Surinach, S.; Kiminami, C.S.; Botta, W.J.; Peres, M.M.; Jorge Junio, A.M. 2Mg-Fe alloys processed by hot-extrusion: influence of processing temperature and the presence of MgO and MgH_2 on hydrogenation sorption properties. *J. Alloys Compd.* **2011**, *509*, S460–S463. [CrossRef]

7. Wang, L.; Jiang, J.; Ma, A.; Li, Y.; Song, D.A. critical review of mg-based hydrogen storage materials processed by equal channel angular pressing. *Metals* **2017**, *7*, 324. [CrossRef]

8. Xiao, X.; Xu, C.; Shao, J.; Zhang, L.; Qin, T.; Li, S.; Ge, H.; Wang, Q.; Chen, L. Remarkable hydrogen desorption properties and mechanisms of the $Mg_2FeH_6@MgH_2$ core-shell nanostructure. *J. Mater. Chem. A* **2015**, *3*, 5517–5524. [CrossRef]

9. Bogdanović, B.; Reiser, A.; Schlichte, K.; Spliethoff, B.; Tesche, B. Thermodynamics and dynamics of the Mg-Fe-H system and its potential for thermochemical thermal energy storage. *J. Alloys Compd.* **2002**, *345*, 77–89. [CrossRef]

10. Crivello, J.-C.; Denys, R.V.; Dornheim, M.; Felderhoff, M.; Grant, D.M.; Huot, J.; Jensen, T.R.; de Jongh, P.; Latroche, M.; Walker, G.S.; et al. Mg-based compounds for hydrogen and energy storage. *Appl. Phys. A* **2016**, *122*, 85. [CrossRef]

11. Urbanczyk, R.; Meggouh, M.; Moury, R.; Peinecke, K.; Peil, S.; Felderhoff, M. Demonstration of Mg_2FeH_6 as heat storage material at temperatures up to 550 °C. *Appl. Phys. A* **2016**, *122*, 315. [CrossRef]

12. Urbanczyk, R.; Peinecke, K.; Peil, S.; Felderhoff, M. Development of a heat storage demonstration unit on the basis of Mg_2FeH_6 as heat storage material and molten salt as heat transfer media. *Int. J. Hydrogen Energy* **2017**, *42*, 13818–13826. [CrossRef]

13. D'Entremont, A.; Corgnale, C.; Sulic, M.; Hardy, B.; Zidan, R.; Motyka, T. Modeling of a thermal energy storage system based on coupled metal hydrides (magnesium iron-sodium alanate) for concentrating solar power plants. *Int. J. Hydrogen Energy* **2017**, *42*, 22518–22529. [CrossRef]

14. Oumellal, Y.; Rougier, A.; Nazri, G.A.; Tarascon, J.-M.; Aymard, L. Metal hydrides for lithium-ion batteries. *Nat. Mater.* **2008**, *7*, 916–921. [CrossRef] [PubMed]

15. Zaïdi, W.; Bonnet, J.-P.; Zhang, J.; Cuevas, F.; Latroche, M.; Couillaud, S.; Bobet, J.; Sougrati, M.T.; Jumas, J.-C.; Aymard, L. Reactivity of complex hydrides Mg_2FeH_6, Mg_2CoH_5 and Mg_2NiH_4 with lithium ion: Far from equilibrium electrochemically driven conversion reactions. *Int. J. Hydrogen Energy* **2013**, *38*, 4798–4808. [CrossRef]

16. Farina, L.; Brutti, S.; Trequattrini, F.; Palumbo, O.; Gatto, S.; Reale, P.; Silvestri, L.; Panero, S.; Paolone, A. An extensive study of the Mg-Fe-H material obtained by reactive ball milling of MgH_2 and Fe in a molar ratio 3:1. *Int. J. Hydrogen Energy* **2017**, *42*, 22333–22341. [CrossRef]

17. Snyder, D.L.; Bish, R.L. *Modern Powder Diffraction*; Bish, D.L., Post, J.E., Eds.; Reviews in Mineralogy & Geochemistry; de Gruyter: Vienna, Austria, 1989; pp. 101–144.

18. Palumbo, O.; Trequattrini, F.; Vitucci, F.M.; Bianchin, A.; Paolone, A. Study of the Hydrogenation/dehydrogenation process in the Mg-Ni-C-Al system. *J. Alloys Compd.* **2015**, *645*, S239–S241. [CrossRef]

19. Palumbo, O.; Brutti, S.; Trequattrini, F.; Sarker, S.; Dolan, M.; Chandra, D.; Paolone, A. Temperature dependence of the elastic modulus of $(Ni_{0.6}Nb_{0.4})_{1-x}Zr_x$ membranes: effects of thermal treatments and hydrogenation. *Energies* **2015**, *8*, 3944–3954. [CrossRef]

20. Witek, K.; Karczewski, K.; Karpowicz, M.; Polanski, M. Mg_2FeH_6 synthesis efficiency map. *Crystals* **2018**, *8*, 94. [CrossRef]

21. Asselli, A.; Huot, J. Investigation of effect of milling atmosphere and starting composition on Mg_2FeH_6 formation. *Metals* **2014**, *4*, 388–400. [CrossRef]

22. Mueller, W.M.; Blackledge, J.P.; Libowitz, G.G. (Eds.) *Metal Hydrides*; Academic Press Inc.: Cambridge, MA, USA, 1968.

23. Peled, E.; Menkin, S. Review-SEI: Past, present and future. *J. Electrochem. Soc.* **2017**, *164*, A1703–A1719. [CrossRef]

24. Zhang, X.; Yang, R.; Qu, J.; Zhao, W.; Xie, L.; Tian, W.; Li, X. The synthesis and hydrogen storage properties of pure nanostructured Mg_2FeH_6. *Nantechnology* **2010**, *21*, 095706. [CrossRef] [PubMed]

25. Meggiolaro, D.; Gigli, G.; Paolone, A.; Vitucci, F.M.; Brutti, S. Incorporation of lithium by MgH_2: An ab initio study. *J. Phys. Chem. C* **2013**, *117*, 22467–22477. [CrossRef]

26. Smith, R.L.; Miser, J.W. *Compilation of the Properties of Lithium Hydride*; 72N74680; NASA Technical Report; NASA: Washington, DC, USA, 1963.

27. Wang, P.; Du, Y.; Liu, S. Thermodynamic optimization of the Li-Mg and Al-Li-Mg systems. *Calphad* **2011**, *35*, 523–532. [CrossRef]

28. Brutti, S.; Mulas, G.; Piciollo, E.; Panero, S.; Reale, P. Magnesium hydride as a high capacity negative electrode for lithium ion batteries. *J. Mater. Chem.* **2012**, *22*, 14531–14537. [CrossRef]

29. Meggiolaro, D.; Gigli, G.; Paolone, A.; Reale, P.; Doublet, M.-L.; Brutti, S. Origin of the voltage hysteresis of MgH2 electrodes in lithium batteries. *J. Phys. Chem. C* **2015**, *119*, 17044–17052. [CrossRef]

30. Silvestri, L.; Farina, L.; Meggiolaro, D.; Panero, S.; Padella, F.; Brutti, S.; Reale, P. Reactivity of sodium alanates in lithium batteries. *J. Phys. Chem. C* **2015**, *119*, 28766–28775. [CrossRef]

31. Laruelle, S.; Grugeon, S.; Poizot, P.; Dollé, M.; Dupont, L.; Tarascon, J.-M. On the Origin of the extra electrochemical capacity displayed by MO/Li cells at low potential. *J. Electrochem. Soc.* **2002**, *149*, A627–A634. [CrossRef]